



Cite this: *Nanoscale*, 2019, **11**, 13725

Received 14th April 2019,
 Accepted 20th June 2019
 DOI: 10.1039/c9nr03203g

rsc.li/nanoscale

Anomalous lattice vibrations of CVD-grown monolayer MoS₂ probed using linear polarized excitation light†

Feng Li,^{‡a} Teng-De Huang,^{‡b} Yann-Wen Lan,^{†b} *^b Ting-Hua Lu,^{*b} Tao Shen,^a
 Kristan Bryan Simbulan^b and Junjie Qi^{†*a}

A novel physical phenomenon and advanced application have been explored in 2D low-dimensional van der Waals layered materials due to their reduced in-plane symmetry. The light–matter interaction is observed upon rapid characterization of the 2D material's crystal orientation. Here, the effects of the sample's rotation angle and the incident light's linear polarization angle on the Raman scattering of chemical vapor deposition (CVD)-grown monolayer MoS₂ were investigated. The results show that the crystal orientation of monolayer MoS₂ can be distinguished by analyzing the intensity ratio and frequency difference of its two dominant Raman vibration modes. In addition, an increase in the incident light's power intensity causes the Raman peaks to red shift due to the photothermal effect. Strikingly, it was found that, with an increase in the incident linear polarization angle, the out-of-plane A_{1g} phonon mode red shifts, while the in-plane E_{2g}¹ phonon mode blue shifts. The frequency difference consequently decreases from 19.5 cm⁻¹ to 17.4 cm⁻¹. The anomalous lattice vibrations of monolayer MoS₂ originate from the built-in strain introduced by the SiO₂/Si substrate. This work paves the way for the investigation and characterization of 2D MoS₂, providing further understanding of the light–matter interaction in 2D materials, which is beneficial for advanced studies on anisotropic MoS₂ based electronic and photoelectric information technologies and sensing applications.

Introduction

Atomic thin transition metal dichalcogenide (TMDC) semiconductors have broad application prospects in electronic devices in virtue of their unique structure and properties.^{1–3}

Strong spin–orbit coupling,^{4,5} the piezoelectric effect,^{6,7} and the exciton Hall effect⁸ were discovered in two dimensional (2D) MoS₂ due to its broken inversion symmetry, which provided a new avenue for exploring novel electronic device concepts. For instance, the emergence of valleytronics utilizing internal degrees of freedom of electrons in 2D broken symmetry crystals holds a great prospect for future electronics.^{9,10}

Raman spectroscopy is a simple, efficient, and nondestructive technique that is widely used in the characterization analysis of 2D materials.^{11–15} It is used to characterize crystal structures, electronic band structures, lattice vibrations, the number of layers, defect densities, strain, *etc.* Recently, studies related to the crystalline orientation and symmetry of 2D materials by controlling the polarization of incident photons in Raman spectroscopy have attracted more and more attention. The zigzag and armchair crystalline directions of black phosphorus and the symmetrical structure of WTe₂ can be identified by using angle-resolved polarized Raman spectroscopy.^{16,17} Both vertical and in-plane orientations of low symmetry triclinic ReS₂ can be distinguished by employing the same polarized Raman microscopy.¹⁸ A further study shows that circularly polarized light leads to a large circular intensity differential in the Raman spectra of layered ReS₂.¹⁹ The helicity-resolved Raman scattering of TMDC atomic layers is more advantageous in distinguishing and assigning phonon modes, and in providing new insights into the relationship between photon helicity and valley polarization.²⁰ The effects of crystalline orientation and polarized excitation light on Raman scattering of CVD grown monolayer MoS₂ have not yet been reported.

In this work, the Raman scattering of CVD-grown monolayer MoS₂ at different crystal orientations was investigated and the association between the crystal and its corresponding Raman shift was established. The effects of power intensity and the excitation light's linear polarization angle on Raman scattering in monolayer MoS₂ were studied, likewise the anomalous lattice vibrations of monolayer MoS₂ were observed. The

^aSchool of Materials Science and Engineering, University of Science and Technology Beijing, Beijing, 100083, People's Republic of China. E-mail: junjieqi@ustb.edu.cn

^bDepartment of Physics, National Taiwan Normal University, Taipei 11677, Taiwan. E-mail: ywlan@ntnu.edu.tw, thlu@ntnu.edu.tw

†Electronic supplementary information (ESI) available. See DOI: 10.1039/c9nr03203g

‡These authors contributed equally to the work.

results presented are significant in the study of the light and matter interaction.

Results

Monolayer MoS₂ samples were synthesized on a silicon wafer coated with 300 nm SiO₂ by a chemical vapor deposition method, for details see the “Experimental section”. Fig. 1a shows the optical image of a representative monolayer MoS₂ which is a triangular flake with about 15 μm edge length. The equilateral geometry of the triangles suggests the monocrystalline feature of monolayer MoS₂.²¹ The photoluminescence (PL) spectra in Fig. 1b show that the optical energy gap of the MoS₂ is about 1.82 eV, revealing its monolayer nature. The surface morphology was analysed on a Bruker Dimension Icon, and the AFM topography (Fig. 1c) of the MoS₂ sample shows a high level surface uniformity that is well combined with the substrate. The step height profile in Fig. 1d indicates the thickness of the triangular MoS₂ at approximately 0.8 nm, further confirming its monolayer character. Fig. 1e illustrates the structure of the optical path of the Raman scattering measurements. As shown in the scheme, a different orientation of linear polarization of 532 nm (~2.33 eV) incident light was produced using a linear polarizer and a half wave plate.

The symmetry of monolayer MoS₂ is broken into specific lattice orientations because of the absence of an inversion center. The crystal in the zigzag direction is symmetric, while in the armchair direction, it is asymmetric.²² The optical images of triangular monolayer MoS₂ in Fig. 2a–c show the sample’s rotation angles between 60° and 90°. According to ref. 20, the rotation angles of 60° and 90° correspond to a zigzag and an armchair orientation along the *x*-axis (the red arrow direction), respectively. Here, the polarization angle of

light is fixed at the horizontal axis, which is shown by red arrows in Fig. 2a–c. The Raman spectra of the out-of-plane A_{1g} vibration and the in-plane E_{2g}¹ vibration are shown in Fig. 2d. In order to obtain the exact intensity and location of the Raman peaks, the Raman peaks are fitted, as shown in Fig. S1†, by using the Gaussian function, which have the standard error of 0.05–0.10 cm⁻¹. The effect of the rotation angle on the intensity and frequency of the two MoS₂ Raman peaks is shown in Fig. S2a and S2b.† Interestingly, as the sample’s rotation angle increases, the E_{2g}¹ mode blue shifts and the A_{1g} mode red shifts. The opposite variation results in a decrease in the Raman frequency difference between the two Raman modes, which is shown in Fig. 2e, where the frequency difference decreases from 21.1 cm⁻¹ to 19.6 cm⁻¹. In addition, the IA_{1g}/IE_{2g}¹ intensity ratio drops from 1.27 to 1.21 as the sample’s rotation angle increases from 60° to 90°, as shown in Fig. 2f. The above scenario is further investigated on another larger monolayer MoS₂ sample, and the results are shown in Fig. S3.† Here, the variation of the Raman intensity ratio and the frequency difference are consistent with the above results.

The frequency of both the A_{1g} and E_{2g}¹ phonon modes for monolayer MoS₂ is not dependent on the crystalline orientation in theory,²³ however the CVD-grown monolayer MoS₂ on the SiO₂/Si substrate experiences about 0.4% intrinsic built-in tensile strain, which leads to its anisotropic properties.²⁴ This anisotropy is due to a strain difference between the armchair and the zigzag orientations due to their distinct structures. It is reported that the phonon mode frequency difference increases with increasing tensile strain,^{23,25,26} so a large frequency difference measured in the zigzag orientation originates from the large strain. Nevertheless, the relation of the peak intensity is irregular in these references. Our results display a lower frequency difference with a higher peak intensity as shown in Fig. S2 and S3.†

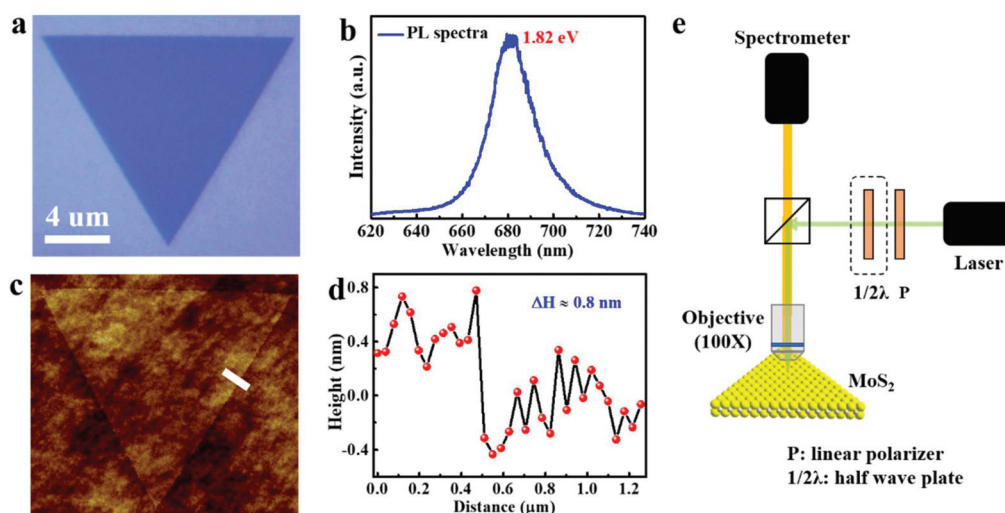


Fig. 1 Characterization of monolayer MoS₂. (a) The OM image of a triangular monolayer MoS₂. (b) The PL spectra of the MoS₂. (c) The AFM topography of the MoS₂. (d) The step height profile along the white line in the AFM image which confirmed the MoS₂ thickness to be about 0.8 nm. (e) Measurement setup of a Raman spectrometer.

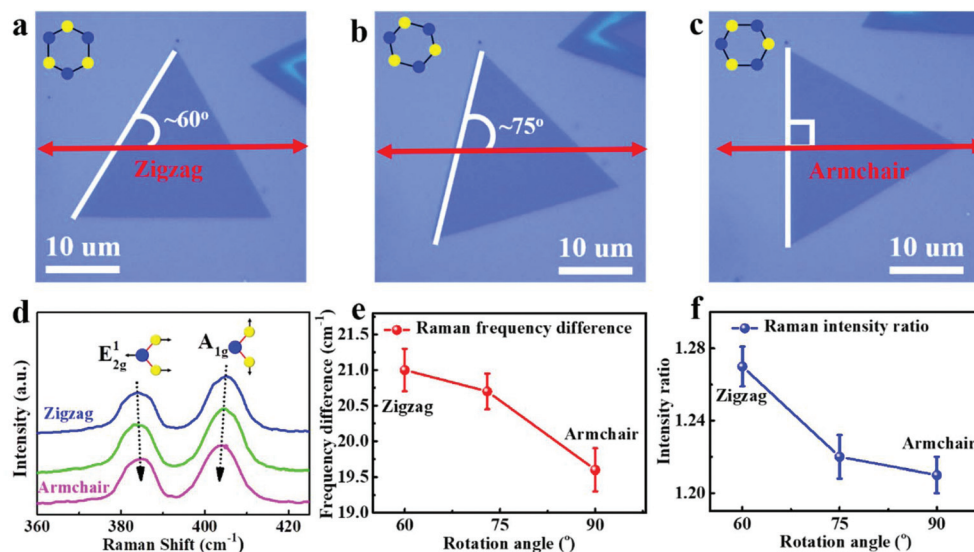


Fig. 2 Effect of varying the crystal orientation of a monolayer MoS₂ to the Raman scattering measurement. (a–c) The optical image of monolayer MoS₂ at different rotation angles (60°, 75° and 90°), with insets showing the direction of the crystal lattice, and (d) the corresponding Raman spectra. The rotation angles at 60° and 90° correspond respectively to the zigzag and armchair crystal orientations along the x-axis. (e) The Raman frequency difference and (f) intensity ratio of the E_{2g}¹ and A_{1g} peaks as a function of the sample's rotation angle.

The optical absorption of MoS₂ irradiated with a laser with E_γ excitation energy can be evaluated by the equation below,²⁷

$$\alpha(\vec{k}, E_\gamma) = \frac{2\pi}{\hbar} \sum_{c,v} |M(c, v, \vec{k})|^2 \delta(\epsilon_c(\vec{k}) - \epsilon_v(\vec{k}) - E_\gamma) \quad (1)$$

in which $\epsilon_c(\vec{k})$ and $\epsilon_v(\vec{k})$ are the electronic band dispersion relation of the conduction and valence bands, respectively, $M(c, v, \vec{k})$ is the electron–photon matrix element, and \hbar is the reduced Planck constant. The optical absorption of MoS₂ at different excitation laser powers (I) and polarization (\vec{P}) can be evaluated by the equation below,

$$I = \frac{2\pi e^2 \hbar^3 I}{m^2 c \epsilon_0} \sum_{c,v} \left| \frac{D(c, v, \vec{k}) \vec{P}}{E_\gamma} \right|^2 \delta(\epsilon_c(\vec{k}) - \epsilon_v(\vec{k}) - E_\gamma) \quad (2)$$

where e is the electronic charge, m is the electron mass, ϵ_0 is the dielectric constant for vacuum and $D(c, v, \vec{k})$ is the dipole vector.

In quantum theory, the Raman intensity of monolayer MoS₂ as a function of the excitation laser energy E_L can be calculated by the equation below,²⁸

$$I = \left| \sum_{i,m,m'} \frac{\langle f | \nabla | m' \rangle \langle m' | H_{\text{el-ph}} | m \rangle \langle m | \nabla | i \rangle}{(E_L - \Delta E_{mi})(E_L - \hbar\omega_V - \Delta E_{mi})} \right|^2 \quad (3)$$

where the matrix elements of $\langle m | \nabla | i \rangle$, $\langle m' | H_{\text{el-ph}} | m \rangle$ and $\langle f | \nabla | m' \rangle$ correspond to the electron–photon of the optical absorption, electron–phonon interaction, and electron–photon of the optical emission, respectively. ΔE_{mi} are the differences of energies between the initial and intermediate states.

The intensity of the in-plane E_{2g}¹ vibration is associated with the band-to-band transition and the high energy excitonic

transition,²⁹ which depends on the phonon and the exciton symmetries.³⁰ In our results, shown in Fig. S2a,† the intensities of E_{2g}¹ for the 60° and 90° rotation angles are 1343.5 and 1430.2 (86.7 difference), respectively, while for A_{1g}, the intensities are 1702.8 and 1732.7 (29.9 difference). This reveals that the changing intensity ratio stems from the asymmetric phonon and exciton properties in strained monolayer MoS₂.

We also investigated the effect of the excitation light's power on the Raman spectrum of monolayer MoS₂, the results of which are displayed in Fig. 3. The laser power was modulated with a graduated neutral-density filter. Fig. 3a shows the Raman spectra of monolayer MoS₂ recorded under different

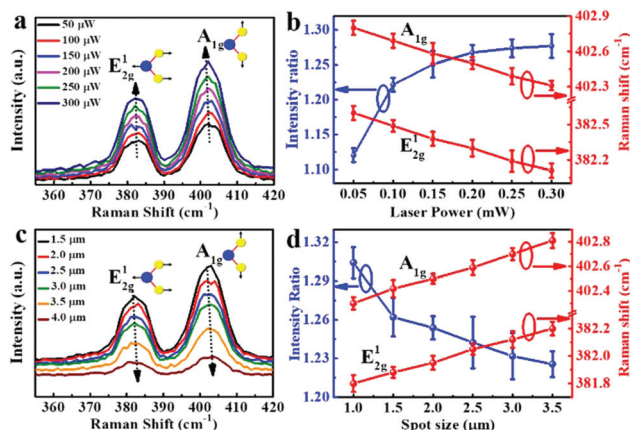


Fig. 3 Effect of excitation laser power density on Raman scattering of monolayer MoS₂. The Raman spectra measured at a different excitation laser power (a) and spot size (c). The Raman shift (red line) and intensity ratio (blue line) of E_{2g}¹ and A_{1g} peaks as a function of excitation laser power (b) and spot size (d).

powers of excitation light. The intensity and intensity ratio of the two MoS₂ Raman peaks are enhanced with the increase in laser power. Both the A_{1g} and E_{2g}¹ vibration modes exhibit an approximately linear reduction, as illustrated by the red line in Fig. 3b (the Raman shift vs. excitation light power plot). Also, red shifts from 402.8 cm⁻¹ to 402.3 cm⁻¹ for A_{1g} and 382.6 cm⁻¹ to 382.1 cm⁻¹ for E_{2g}¹ were observed with an increase in the laser power from 0.05 mW to 0.30 mW. Note that the frequency difference between the two peaks is almost unchanged, keeping at a value of 20.2 cm⁻¹. In addition, the effect of the excitation laser spot size on the Raman scattering of monolayer MoS₂ was also investigated. With a fixed 0.3 mW laser power, the spot size of the incident laser was varied by tuning the sample stage to defocus the light beam. The optical image of the series laser beam is shown in Fig. S4,† while the corresponding Raman results are shown in Fig. 3c. The intensity and intensity ratio of the two peaks are lowered down as the spot size widens, resulting in a blue shift in the A_{1g} and E_{2g}¹ peaks (Fig. 3d). Obviously, the increase in laser power as well as the shrinking of the spot size causes the power density to increase.

The shift of both Raman peaks stems from thermal expansion and temperature by the laser heating effect. The Raman shifts of monolayer MoS₂ at different temperatures in ref. 31–33 are consistent with our results. The phonon frequency ω can be expressed as a function of volume and temperature,³³

$$\left(\frac{\partial \ln \omega}{\partial T}\right) = \left(\frac{\partial \ln V}{\partial T}\right)_P \left(\frac{\partial \ln \omega}{\partial \ln V}\right)_T + \left(\frac{\partial \ln \omega}{\partial T}\right)_V. \quad (4)$$

The ω of both vibration modes red shifts with the increase in temperature and the decrease in spot size as inferred from the above equation. In addition, the red shift of A_{1g} and E_{2g}¹ modes with increased excitation light power is also observed in the NiFe₂O₄ film. They believe that the shift of the phonon frequency is due to the disorder induced by thermal effects.³⁴ In ref. 32, the temperature coefficients of A_{1g} and E_{2g}¹ modes are -0.0132 and -0.0123 cm⁻¹/°C, respectively, which implies that the frequency difference can also be changed by a large excitation power.

The enhancement of intensity is due to the improvements in optical absorption as the temperature increases, which can easily be inferred from eqn (2) and have been experimentally investigated using the light absorption spectrum.³³ Exciton-phonon coupling is also enhanced with increasing laser power. Meanwhile, the increase in the peak intensity ratio with the increase of laser power density is caused by the higher rate of change of A_{1g} compared to that of the E_{2g}¹ phonon mode, as shown in Fig. S5.† The difference between the two phonon modes is derived from the distinct properties along the in-plane (E_{2g}¹) and the out-of-plane (A_{1g}) in monolayer MoS₂. Owing to this reason, the electron-phonon coupling (which is associated with temperature) for A_{1g} is stronger than for E_{2g}¹.³⁵

A fixed power is then employed while changing the linear polarization angle of the excitation light using a linear polarizer and a half-wave plate in the Raman spectrometer. The

effect of the linear polarization angle on the Raman scattering of monolayer MoS₂ was studied. The Raman spectra of monolayer MoS₂ measured at polarization angles from 0° to 90° are shown in Fig. 4a. Strikingly, with the increase of the excitation light's linear polarization angle, the A_{1g} phonon mode stiffens (red shifts), while the E_{2g}¹ phonon mode softens (blue shifts). The frequency of the A_{1g} phonon mode decreases from 404.6 cm⁻¹ to 404.1 cm⁻¹ while that of the E_{2g}¹ phonon mode increases from 385.1 cm⁻¹ to 386.7 cm⁻¹, and the rate of frequency change is over three times larger for E_{2g}¹ compared to that for A_{1g}, as shown in Fig. S6a.† The frequency difference between the two modes decreases from 19.5 cm⁻¹ to 17.4 cm⁻¹ (as shown in Fig. 4b), a reduction of 2.1 cm⁻¹. A similar result is also observed in another sample as shown in Fig. S7.† In order to emphasize their differences, only two Raman spectra measured under 0° and 90° linear polarization are presented. Here, the frequency difference of the two MoS₂ Raman peaks decreases from 19.9 cm⁻¹ to 17.9 cm⁻¹, while no shift is observed in the Raman peak of silicon.

The effect of the linear polarization angle is similar to the effect of the rotation angle and the sample thickness. The anomalous behavior of Raman scattering in monolayer MoS₂ probed by linear polarized light is similar to the one affected by the thickness effect and behaves differently from the ones under the influence of temperature and laser power density. This reveals why the frequency difference of monolayer MoS₂ is discrepantly measured by using different Raman spectrometers. The Raman frequency difference of monolayer MoS₂ from various references is in the range of 17.1 cm⁻¹–21.0 cm⁻¹, and the typical results are displayed in Fig. 5. In our results, the Raman frequency of the same monolayer MoS₂ can be between 17.4 cm⁻¹ and 21.1 cm⁻¹ at different rotation angles and at different linear polarization angles of the excitation light. The variation in the Raman frequency difference is due to the anisotropy of the light-matter interaction, *i.e.* small and large differences correspond to the small and large strain, respectively.

In addition, with the increase of the linear polarization angle of the excitation, the I_{A1g}/I_{E2g}¹ intensity ratio is improved to a maximum value (1.53) at 90°, see the blue line in Fig. 4b. The intensity ratio is probably affected by the aniso-

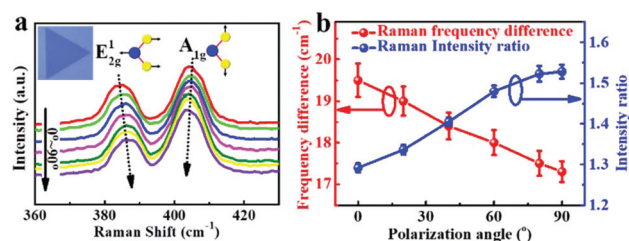


Fig. 4 Effect of linearly polarized excitation light on the Raman scattering of monolayer MoS₂. (a) The Raman spectra of an armchair direction sample. (b) The Raman frequency difference (red line) and intensity ratio (blue line) of E_{2g}¹ and A_{1g} peaks as a function of linear polarization angle.

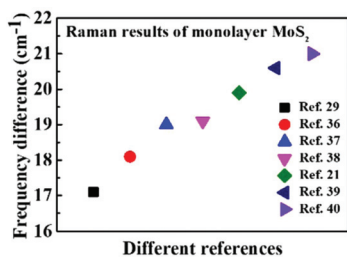


Fig. 5 The typical Raman frequency difference of monolayer MoS₂ as reported in various references.

tropic material, which could induce a different electron-phonon coupling strength. A higher intensity means a higher intensity ratio, which is consistent with the effect of laser power density. Similar results have also been demonstrated in monolayer MoS₂ nanoribbons, which stemmed from the anisotropy of its armchair and zigzag crystal orientations.⁴¹ In this work, the monolayer MoS₂, grown by a CVD method on a SiO₂/Si substrate, has built-in tensile strain which causes its anisotropic properties.

There are many factors that affect the locations and intensities of the two vibrational modes of monolayer MoS₂. First of all, the frequencies of the A_{1g} and E_{2g}¹ phonon modes shift in opposite directions under the influence of disorders,⁴² the sample's rotation angle, and the linear polarization angle of the excitation light. The frequency of the A_{1g} phonon mode is sensitive to electron doping³⁵ and environment (vacuum, ambient and DI water),⁴² while the E_{2g}¹ phonon mode is sensitive to strain.^{23,25,26} Both frequencies of the A_{1g} and the E_{2g}¹ phonon modes shift to the same direction, which is attributable to the effects of temperature and laser power. Meanwhile, both A_{1g} and E_{2g}¹ intensities vary under the influence of disorders,⁴² temperature,^{31–33} laser power, the sample's rotation angle and the linear polarization angle of the excitation light, while their intensities vary oppositely to the effects of electron doping and the environment. Our investigations on the variations of the Raman peaks' intensity ratio and frequency difference provide a new insight to explain why the Raman frequency difference of monolayer MoS₂ shows discrepancy in various studies.

Conclusions

In conclusion, the effects of the rotation angle, power, and linear polarization angle of the excitation light on the Raman spectrum of CVD-grown monolayer MoS₂ were investigated. When the crystal orientation of monolayer MoS₂ changes from the zigzag direction to the armchair direction along the *x*-axis, the frequency difference between A_{1g} and E_{2g}¹ vibration modes decreases from 21.1 cm⁻¹ to 19.6 cm⁻¹ and the I_{A_{1g}}/I_{E_{2g}¹} intensity ratio also decreases from 1.27 to 1.21. The Raman peaks red shift with the increase in the excited light's power intensity. Moreover, with the increase of the incident light's

linear polarization angle, the frequency difference between the two modes drops from 19.5 cm⁻¹ to 17.4 cm⁻¹, that is a reduction by 2.1 cm⁻¹, and the intensity ratio increases from 1.27 at 0° to a maximum value of 1.53 at 90°.

Experimental details

Sample preparation

2D MoS₂ samples were grown inside a three-temperature zone tube furnace equipped with a 60 mm diameter quartz tube. The synthesis process was similar to the processes described in refs. 43 and 44. The Si/SiO₂ substrates were cleaned in acetone, alcohol, and deionized water. The dried MoO₃ powder (10 mg) was placed on a quartz boat located at the center of the third furnace zone downstream of the carrier gas. The 2 cm × 2 cm Si/SiO₂ substrate used for growing MoS₂ was placed face-down above the MoO₃ powder. The S powders were placed in a ceramic boat located at the center of the first furnace zone at the upper stream. The S powders were heated to an approximate temperature of 160–180 °C before MoO₃ was heated to about 850 °C at 25 °C min⁻¹. The S and MoO_{3-x} vapors were brought to the target substrate by an ultrahigh-purity Ar carrier gas of 100 sccm. The growth recipe was allowed to sit for 30 min before being cooled inside the furnace to room temperature.

Raman measurement system

Raman spectra were obtained using a JY Horiba HR800 equipped with a liquid nitrogen cooled CCD, a Nd:YAG 532 nm solid state excitation laser and an optical microscope. The laser power was below 1 mW to avoid damage to the MoS₂ samples. Before obtaining the Raman spectra, the surface morphologies of 2D MoS₂ were examined with the optical microscope. A 100× objective lens was used to focus the laser and collect the Raman scattered light, and an 1800 lines per mm grating was chosen for spectra acquisition. A linear polarizer and a half-wave plate were placed in the incident light path to obtain linearly polarized light.

Conflicts of interest

There are no conflicts to declare.

Acknowledgements

This work was supported by the National Natural Science Foundation of China (No. 51572025), the National Foundation of China (No. 41422050303), the Beijing Municipal Science & Technology Commission, and the Fundamental Research Funds for Central Universities. This work was also supported by the National Science Council, Taiwan under contract No. MOST 105-2112-M-003-016-MY3 and MOST 107-2112-M-003-012.

Notes and references

- Q. H. Wang, K. Kalantar-Zadeh, A. Kis, J. N. Coleman and M. S. Strano, *Nat. Nanotechnol.*, 2012, **7**, 699–712.
- M. Xu, T. Liang, M. Shi and H. Chen, *Chem. Rev.*, 2013, **113**, 3766–3798.
- C. Tan, X. Cao, X. J. Wu, Q. He, J. Yang, X. Zhang, J. Chen, W. Zhao, S. Han, G. H. Nam, M. Sindoro and H. Zhang, *Chem. Rev.*, 2017, **117**, 6225.
- D. Xiao, G. B. Liu, W. Feng, X. Xu and W. Yao, *Phys. Rev. Lett.*, 2012, **108**, 196802.
- Z. Y. Zhu, Y. C. Cheng and U. Schwingenschlog, *Phys. Rev. B: Condens. Matter Mater. Phys.*, 2011, **84**, 153402.
- W. Wu, L. Wang, Y. Li, F. Zhang, L. Lin, S. Niu, D. Chenet, X. Zhang, Y. Hao, T. F. Heinz, J. Hone and Z. L. Wang, *Nature*, 2014, **514**, 470.
- J. Qi, Y. W. Lan, A. Z. Stieg, J. H. Chen, Y. L. Zhong, L. J. Li, C. D. Chen, Y. Zhang and K. L. Wang, *Nat. Commun.*, 2015, **6**, 7430.
- M. Onga, Y. Zhang, T. Ideue and Y. Iwasa, *Nat. Mater.*, 2017, **16**, 1193.
- H. Zeng, J. Dai, W. Yao, D. Xiao and X. Cui, *Nat. Nanotechnol.*, 2012, **7**, 490–493.
- N. Zibouche, P. Philippsen, A. Kuc and T. Heine, *Phys. Rev. B: Condens. Matter Mater. Phys.*, 2014, **90**, 125440.
- X. Zhang, Q. H. Tan, J. B. Wu, W. Shi and P. H. Tan, *Nanoscale*, 2016, **8**, 6435.
- J. U. Lee, M. Kim and H. Cheong, *Appl. Microsc.*, 2015, **45**, 126.
- W. M. Parkin, A. Balan, L. Liang, P. M. Das, M. Lamparski, C. H. Naylor, J. A. Rodríguez-Manzo, A. T. C. Johnson, V. Meunier and M. Drndic, *ACS Nano*, 2016, **10**, 4134.
- C. Lee, H. Yan, L. E. Brus, T. F. Heinz, J. Hone and S. Ryu, *ACS Nano*, 2010, **4**, 2695.
- M. Rahaman, R. D. Rodriguez, G. Plechinger, S. Moras, C. Schuller, T. Korn and D. R. T. Zahn, *Nano Lett.*, 2017, **17**, 6027.
- J. Wu, N. Mao, L. Xie, H. Xu and J. Zhang, *Angew. Chem.*, 2015, **127**, 2396.
- Q. Song, X. Pan, H. Wang, K. Zhang, Q. Tan, P. Li, Y. Wan, Y. Wang, X. Xu, M. Lin, X. Wan, F. Song and L. Dai, *Sci. Rep.*, 2016, **6**, 29254.
- L. Hart, S. Dale, S. Hoyer, J. L. Webb and D. Wolverson, *Nano Lett.*, 2016, **16**, 1381.
- S. Zhang, N. Mao, N. Zhang, J. Wu, L. Tong and J. Zhang, *ACS Nano*, 2017, **11**, 10366.
- S. Y. Chen, C. Zheng, M. S. Fuhrer and J. Yan, *Nano Lett.*, 2015, **15**, 2526.
- S. Najmaei, Z. Liu, W. Zhou, X. Zou, G. Shi, S. Lei, B. I. Yakobson, J. C. Idrobo, P. M. Ajayan and J. Lou, *Nat. Mater.*, 2013, **12**, 754.
- A. M. van der Zande, P. Y. Huang, D. A. Chenet, T. C. Berkelbach, Y. You, G. H. Lee, T. F. Heinz, D. R. Reichman, D. A. Muller and J. C. Hone, *Nat. Mater.*, 2013, **12**, 554.
- D. Doratotaj, J. R. Simpson and J. A. Yan, *Phys. Rev. B*, 2016, **93**, 075401.
- W. H. Chae, J. D. Cain, E. D. Hanson, A. A. Murthy and V. P. Dravid, *Appl. Phys. Lett.*, 2017, **111**, 143106.
- S. J. R. Tan, S. Sarkar, X. Zhao, X. Luo, Y. Z. Luo, S. M. Poh, I. Abdelwahab, W. Zhou, T. Venkatesan, W. Chen, S. Y. Quek and K. P. Loh, *ACS Nano*, 2018, **12**, 5051.
- H. Li, A. W. Contryman, X. Qian, S. M. Ardakani, Y. Gong, X. Wang, J. M. Weisse, C. H. Lee, J. Zhao, P. M. Ajayan, J. Li, H. C. Manoharan and X. Zheng, *Nat. Commun.*, 2015, **6**, 7381.
- H. L. Liu, H. Guo, T. Yang, Z. Zhang, Y. Kumamoto, C. Chiang Shen, Y. T. Hsu, L. J. Li, R. Saitob and S. Kawatadg, *Phys. Chem. Chem. Phys.*, 2015, **17**, 14561.
- R. Saito, Y. Tatsumi, S. Huang, X. Ling and M. S. Dresselhaus, *J. Phys.: Condens. Matter*, 2016, **28**, 35.
- D. Y. Qiu, F. H. da Jornada and S. G. Louie, *Phys. Rev. Lett.*, 2013, **111**, 216805.
- B. R. Carvalho, L. M. Malard, J. M. Alves, C. Fantini and M. A. Pimenta, *Phys. Rev. Lett.*, 2015, **114**, 136403.
- S. Sahoo, A. P. S. Gaur, M. Ahmadi, M. J. F. Guinel and R. S. Katiyar, *J. Phys. Chem. C*, 2013, **117**, 9042.
- N. A. Lanzillo, A. G. Birdwell, M. Amani, F. J. Crowne, P. B. Shah, S. Najmaei, Z. Liu, P. M. Ajayan, J. Lou, M. Dubey, S. K. Nayak and T. P. O'Regan, *Appl. Phys. Lett.*, 2013, **103**, 093102.
- E. Yalon, Ö. B. Aslan, K. K. H. Smithe, C. J. McClellan, S. V. Suryavanshi, F. Xiong, A. Sood, C. M. Neumann, X. Xu, K. E. Goodson, T. F. Heinz and E. Pop, *ACS Appl. Mater. Interfaces*, 2017, **9**, 43013.
- A. Ahlawat and V. G. Sathe, *J. Raman Spectrosc.*, 2011, **42**, 1087.
- B. Chakraborty, A. Bera, D. V. S. Muthu, S. Bhowmick, U. V. Waghmare and A. K. Sood, *Phys. Rev. B: Condens. Matter Mater. Phys.*, 2012, **85**, 161403.
- J. Yan, J. Xia, X. Wang, L. Liu, J. L. Kuo, B. K. Tay, S. Chen, W. Zhou, Z. Liu and Z. X. Shen, *Nano Lett.*, 2015, **15**, 8155.
- H. Qiu, T. Xu, Z. Wang, W. Ren, H. Nan, Z. Ni, Q. Chen, S. Yuan, F. Miao, F. Song, G. Long, Y. Shi, L. Sun, J. Wang and X. Wang, *Nat. Commun.*, 2013, **4**, 2642.
- C. Lee, H. Yan, L. E. Brus, T. F. Heinz, J. Hone and S. Ryu, *ACS Nano*, 2010, **4**, 2695.
- J. Shi, D. Ma, G. F. Han, Y. Zhang, Q. Ji, T. Gao, J. Sun, X. Song, C. Li, Y. Zhang, X. Y. Lang, Y. Zhang and Z. Liu, *ACS Nano*, 2014, **8**, 10196.
- H. Schmidt, S. Wang, L. Chu, M. Toh, R. Kumar, W. Zhao, A. H. C. Neto, J. Martin, S. Adam, B. özyilmaz and G. Eda, *Nano Lett.*, 2014, **14**, 1909.
- J. B. Wu, H. Zhao, Y. Li, D. Ohlberg, W. Shi, W. Wu, H. Wang and P. H. Tan, *Adv. Opt. Mater.*, 2016, **4**, 756.
- U. Wurstbauer, B. Miller, E. Parzinger and A. W. Holleitner, *J. Phys. D: Appl. Phys.*, 2017, **50**, 173001.
- F. Li, J. Qi, M. Xu, J. Xiao, Y. Xu, X. Zhang, S. Liu and Y. Zhang, *Small*, 2017, **13**, 1603103.
- F. Li, Z. Lu, Y. W. Lan, L. Jiao, M. Xu, X. Zhu, X. Zhang, H. Wu and J. Qi, *Nanotechnology*, 2018, **29**, 275202.